Biomaterials Science

PAPER

View Article Online
View Journal | View Issue

Cite this: *Biomater. Sci.*, 2017, **5**, 2144

3D printed poly(ε-caprolactone) scaffolds modified with hydroxyapatite and poly(propylene fumarate) and their effects on the healing of rabbit femur defects†

Senem Buyuksungur,[a,b] Tugba Endogan Tanir,[a,c] Arda Buyuksungur,[a] Ezgi Irem Bektas,[d] Gamze Torun Kose,[a,d] Deniz Yucel,[a,e] Tahsin Beyzadeoglu,[f] Engin Cetinkaya,[g] Cagri Yenigun,[h] Ergin Tönük, [a,h,i] Vasif Hasirci *[a,b,i,j] and Nesrin Hasirci *[a,b,i,k]

A large variety of approaches have been used to treat large and irregular shaped bone defects with less than optimal success due to material or design issues. In recent years patient specific constructs prepared by additive manufacturing provided a solution to the need for shaping implants to fit irregular defects in the surgery theater. In this study, cylindrical disks of poly(ε-caprolactone) (PCL) were printed by fused deposition modeling and modified with nanohydroxyapatite (HAp) and poly(propylene fumarate) (PPF) to create a mechanically strong implant with well-defined pore size and porosity, controllable surface hydrophilicity (with PPF) and osteoconductivity (with HAp). Cytotoxicity, irritation and inflammation tests demonstrated that the scaffolds were biocompatible. PCL/HAp and PCL/HAp/PPF scaffolds were implanted in the femurs of rabbits with and without seeding with rabbit Bone Marrow Stem Cells (BMSC) and examined after 4 and 8 weeks with micro-CT, mechanically and histologically. BMSC seeded PCL/HAp/PPF scaffolds showed improved tissue regeneration as determined by bone mineral density and micro-CT. Compressive and tension stiffness values (394 and 463 N mm^{-1}) were significantly higher than those of the healthy rabbit femur (316 and 392 N mm^{-1}, respectively) after 8 weeks of implantation. These 3D implants have great potential for patient-specific bone defect treatments.

Received 13th June 2017,
Accepted 14th August 2017

DOI: 10.1039/c7bm00514h

rsc.li/biomaterials-science

1. Introduction

In the United States, there are more than two million people suffering from orthopedic problems and about 800 000 bone graft procedures are carried out annually with an estimated cost of US$ 17 billion.[1] The best treatment for the bone defects resulting from osteoporosis related fractures, trauma, tumor resection and bone malformation is the application of bone autografts. Although autografts are known as the golden standard they have many drawbacks such as donor site morbidity, difficulty in harvesting sufficient bone and the pain due to the second surgery. Allografts and xenografts are other options but they have drawbacks including disease transmission, immune reactions and donor scarcity.

Particularly in the case of craniofacial defects bone grafting involves extensive reshaping, and the final outcome is not always satisfactory for the patients and the surgeons. Patient specific customized tissue engineered constructs with desired shapes and dimensions which would fit the defect perfectly would be the ideal solution for these problems.[2,3] Bone tissue engineering which combines scaffolds, cells, and/or bioactive agents such as growth factors is a developing strategy to develop bone substitutes having osteoconductivity, osteoinductivity and osteogenesis. This would solve the problems due to donor scarcity and the need for autografts. An ideal scaffold, a cell carrier, should have structural and mechanical properties

[a]*Middle East Technical University (METU), BIOMATEN Center of Excellence in Biomaterials and Tissue Engineering, Ankara, Turkey. E-mail: nhasirci@metu.edu.tr*
[b]*METU, Graduate Department of Biotechnology, Ankara, Turkey*
[c]*METU Central Laboratory, Ankara, Turkey*
[d]*Genetics and Bioengineering Department, Yeditepe University, Istanbul, Turkey*
[e]*Department of Histology and Embryology, School of Medicine, Acibadem University, Istanbul, Turkey*
[f]*Department of Orthopaedics and Traumatology, Faculty of Health Sciences, Haliç University, Istanbul, Turkey*
[g]*Baltalimani Bone Diseases Training and Research Hospital, Sarıyer, Istanbul, Turkey*
[h]*METU, Department of Mechanical Engineering, Ankara, Turkey*
[i]*METU, Graduate Department of Biomedical Engineering, Ankara, Turkey*
[j]*METU, Department of Biological Sciences, Ankara, Turkey*
[k]*METU, Department of Chemistry, Ankara, Turkey*
†Electronic supplementary information (ESI) available. See DOI: 10.1039/c7bm00514h

similar to that of the natural bone, and have a highly porous structure with interconnected pores which would allow the exchange of nutrients, oxygen and metabolic waste products as well as movement of cells within its structure. In the earlier stages of tissue engineering, sponges and fibrous structures were used to serve as the scaffolds but the fit to the defect site remained an unsolved problem.[4] In the last decades, scaffolds specific to the need of the patient have been produced by additive manufacturing, and one of the most promising additive manufacturing techniques is fused deposition modeling (FDM), which results in a highly precise pore size, an ordered structure, predetermined interconnectivity, and a desired shape. These implants are modeled after scanning with computed tomography and printed with different techniques using metals and polymers or composites.

Although metallic implants have the strength needed in a load bearing bone implant, their corrosion risks, non-degradability and low cell–material interactions have made biodegradable polymers preferable for most bone treatments. Poly (lactic acid) (PLA), poly(glycolic acid) (PGA), random copolymers of poly(lactic acid-*co*-glycolic acid) (PLGA) and poly(ε-caprolactone) (PCL) are used in scaffold preparation as biodegradable polymers.[5–7] PCL, which is a biocompatible polymer approved by the FDA (Food and Drug Administration of USA), has been preferred for use in implants, drug delivery devices, suture materials and adhesion barriers due to its good biocompatibility.[8,9] Besides, PCL is an ideal thermoplastic polymer for FDM due to its low melting temperature (60 °C) which leads to easy printability, also maintaining strong crystallization and moderate mechanical properties after manufacturing.[10] But, the use of PCL alone in bone tissue engineering applications is limited due to the feature of non osteoinductivity.[11] In general PCL has been used after functionalization with various forms of calcium phosphate, either by coating onto or incorporating into the scaffolds.[12]

In bone tissue engineering applications stem cells or bone cells are loaded and incubated in the scaffolds. A major deficiency of many polyesters is the lack of functional groups to attract the cells. This is remedied to some extent by the addition of bioactive minerals such as hydroxyapatite (HAp) in the scaffold composition. HAp is found in the natural bone as its major inorganic component (60% of the bone composition) and has been shown to improve the mechanical strength and osteoinductivity when introduced to scaffolds.[13,14] The presence of HAp stimulates the deposition of calcium phosphate and that results in enhanced bone-substrate interface strength.[15] Poly(propylene fumarate) (PPF) is another biodegradable polymer that has been used in controlled drug delivery and scaffold preparation for bone tissue engineering.[16,17] PPF degrades *in vivo* to fumaric acid and propylene glycol which can be metabolized as a constituent of the Krebs cycle.[18] Fumaric acid is a key intermediate in the tricarboxylic acid cycle in organic acid biosynthesis in humans and other mammals. Fumaric acid and its esters are also known to have carcinogenesis inhibitory activity, are approved for the treatment of immune-mediated psoriasis disease, and are employed in different areas such as tissue engineering, delivery of active agents, immunology, dermatology, multiple sclerosis, neurology and cancer studies.[19] Meanwhile, PPF has unique mechanical properties suitable for bone tissue engineering applications. An important property of PPF is that it can be crosslinked with various agents easily due to unsaturated bonds in each subunit of PPF thus improving its characteristics.[20]

The goal of the present study was to produce 3D PCL scaffolds by the FDM technique and increase their interaction with cells by coating with HAp and PPF. This would yield a patient specific biodegradable and bioactive composite scaffold for advanced bone tissue engineering applications. The cylindrical PCL scaffolds were produced using a predetermined model, and PCL/HAp and PCL/HAp/PPF composite scaffolds were prepared by coating these structures. Although there are many studies in the literature using PCL and PCL/HAp scaffolds in bone tissue engineering, this is the first study in which the PCL/HAp/PPF composite scaffolds were prepared by additive manufacturing. Scaffolds were produced with different architectures by changing the position of the deposited fibers on successive layers: basic (B) and basic shift (BS) (Fig. 1A). The physical and chemical properties of the scaffolds were characterized by using a stereo microscope, scanning electron microscope (SEM), micro-computed tomography (μ-CT), energy-dispersive X-ray spectroscopy (EDS) and mechanical analysis. In cell culture experiments biocompatibility and stem cell behavior on the scaffolds were investigated under *in vitro* conditions by using L929 fibroblast cells and rabbit bone marrow derived mesenchymal stem cells (BMSCs). Finally, the *in vivo* bone regeneration capability of the scaffolds was assessed after 4 and 8 weeks of orthotopic implantation in femoral defects in rabbits.

2. Materials and methods

2.1 Materials

Poly(ε-caprolactone) (PCL) (MW 80 000 g mol^{-1}), hydroxyapatite (HAp) nanopowder (<200 nm), DRAQ5, FITC-labelled phalloidin, Irgacure 2959, *Pseudomonas* lipase, and fumaric acid, were purchased from Sigma-Aldrich (USA). Trypsin/EDTA and GeneJET RNA purification kits were obtained from Thermo Scientific (USA). Fetal bovine serum (FBS) was obtained from Biowest (France). Alizarin red was obtained from Cyagen. Penicillin/streptomycin (100 U mL^{-1}–100 μg mL^{-1}) was a product of Fluka (Switzerland). Alamar Blue cell proliferation assay solution was from Invitrogen Inc. (USA). Dulbecco's Modified Eagle's Medium (DMEM)-high glucose (glucose concentration: 4.5 g L^{-1}) was from Lonza (Switzerland). Alkaline phosphatase (ALP) kit was obtained from Anaspec (USA). MEM-α (1×) + GlutaMAX™ was purchased from Gibco (USA).

2.2 PCL scaffold fabrication by FDM method

PCL scaffolds were fabricated with Bioscaffolder® (SYS+ENG, Germany). Molten PCL pellets were extruded through a needle

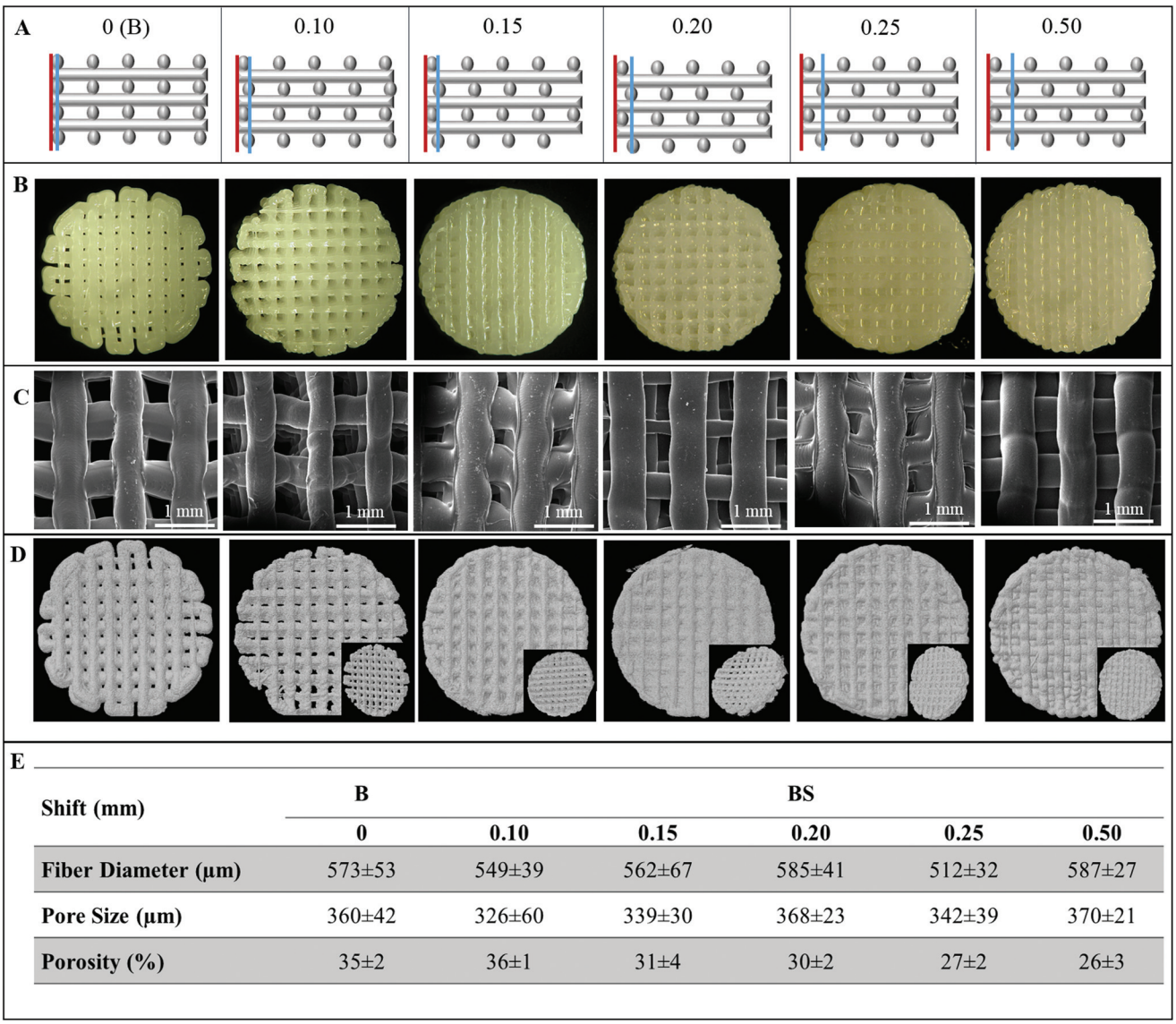

Shift (mm)	B	BS				
	0	0.10	0.15	0.20	0.25	0.50
Fiber Diameter (μm)	573±53	549±39	562±67	585±41	512±32	587±27
Pore Size (μm)	360±42	326±60	339±30	368±23	342±39	370±21
Porosity (%)	35±2	36±1	31±4	30±2	27±2	26±3

Fig. 1 Physical characterization of 3D printed B (0 mm) and BS (shifted 0.10, 0.15, 0.20, 0.25, 0.50 mm) PCL scaffolds. (A) Schematic representations of the PCL scaffolds in cross sectional views. (B) Stereomicrographs, (C) SEM micrographs, and (D) micro-CT of the scaffolds seen from the top. The insets show the models at an angle. (E) Table of fiber diameters, pore size and porosity values of the B and BS scaffolds. The blue lines in (A) indicate the change of localization of the fibers in subsequent layers. Statistical analysis of porosity was carried out by using one-way ANOVA. The porosity differences between B–BS0.25 (*$p < 0.05$), B–BS0.50 (**$p < 0.01$), BS0.10–BS0.25 (**$p < 0.01$), and BS0.10–BS0.50 (**$p < 0.01$) are statistically significant.

(i.d. 210 μm). Cylindrical PCL scaffolds (10 mm diameter and 1.5 mm height for characterization and *in vitro* studies; and 5 mm diameter and 2.5 mm height for *in vivo* studies) were plotted according to a model prepared by Sketchup (Trimble Inc., USA) up to 10 layers. Scaffolds with different architectures were produced by changing the respective orientation of the deposited fibers. 3D PCL scaffolds were produced according to two different architectures, namely: basic (B) and basic shift (BS) structures (Fig. 1A). The B scaffold was produced by the consecutive deposition of two-dimensional (2D) layers which have fibers that are perpendicular to each other. The BS scaffolds with different shifting distances (0.50, 0.25, 0.20, 0.15 and 0.10 mm) were produced similarly, but each 2D layer was deposited within a shift distance relative to the previous layer.

2.3 Composite scaffold preparation

Nanohydroxyapatite (HAp) (5%, w/w) was suspended in dichloromethane (DCM) : acetone (20 : 80, v/v) solution and scaffolds were immersed into this suspension to be coated with the mineral. The solvents were evaporated at room temperature, leaving a layer of hydroxyapatite coating on the scaffold. For the preparation of PCL/HAp/PPF scaffolds, PPF was dissolved in acetone (PPF : acetone, 50 : 50, w/w), Irgacure 2959

(5%, w/w) photoinitiator was added, and HAp was added to yield a 5%, w/w solution. The scaffolds were dip-coated in this suspension and then exposed to UV (365 nm, distance 15 cm, 0.120 joule cm^{-2}) in a UV crosslinker chamber (Bio-Link-UV Crosslinker BLX-365, USA) for 30 min to crosslink the PPF.

2.4 Physical and chemical characterization of 3D scaffolds

2.4.1 Scanning electron microscopy (SEM). Scaffolds were examined by using a Scanning Electron Microscope (SEM, FEI Quanta 400F, The Netherlands) after sputter-coating with gold–palladium (Au–Pd) under argon atmosphere. The chemical compositions of PCL, PCL/HAp and PCL/HAp/PPF scaffolds were analyzed with energy dispersive X-ray spectroscopy (EDS).

2.4.2 Micro-computed tomography (μ-CT). Scaffolds were scanned with μ-CT (Bruker μ-CT, 1172, Belgium) with application of 11 μm per pixel size, using aluminum filters. Samples were rotated 0.7° throughout 360°. Porosity and pore size distributions were calculated by using CTAn software (Bruker μ-CT, Belgium).

2.4.3 Contact angle measurements. Water contact angles (WCA) of the PCL, PCL/HAp and PCL/HAp/PPF scaffolds were measured by the sessile drop method using a goniometer (Attension, Biolin Scientific, Sweden). The measurements were made with distilled water with drop volume of 7 μL.

2.4.4 Mechanical analysis. The mechanical properties of the 3D scaffolds (10 mm diameter and 1.5 mm height) were studied with compression tests by using a Mechanical Tester (Shimadzu AGS-X Universal Test Machine, Japan). The compression speed was 1 mm min^{-1}. The compressive modulus of the scaffolds was calculated from the initial linear elastic region of the stress–strain curves. To study the influence of radiation on mechanical properties, mechanical tests were also applied to the scaffolds which were irradiated with ^{60}Co gamma (dose 25 kGy) for sterilization.

2.4.5 Evaluation of enzymatic degradation *in situ*. The stability of the scaffolds was evaluated by incubating the scaffolds in an aqueous solution of *Pseudomonas* lipase enzyme according to ASTM F-1635. Samples were incubated in a phosphate buffered saline (PBS, 10 mM, pH 7.4) solution of lipase (180 U L^{-1}) at a concentration similar to that in human serum (30–190 U L^{-1}).[21] Sodium azide (0.2%) was added to avoid contamination and the samples were kept at 37 °C up to 35 days under dynamic conditions in an orbital shaker at 70 rpm (Innova 4000 Incubator Shaker, New Brunswick, Germany). The samples were removed periodically, washed with distilled water, freeze dried and weighed to determine the weight loss. Weight loss was calculated as follows:

$$\text{Weight loss } (\%) = [(W_0 - W_1)/W_0] \times 100$$

where W_0 and W_1 are the weights of dry samples before and after degradation, respectively.

2.5 *In vitro* studies

2.5.1 Cytotoxicity of the scaffolds. *In vitro* cytotoxicity tests of scaffolds were performed according to ISO 10993-5. The tests were performed by using extracts of the samples obtained by incubating the scaffolds in complete media (DMEM high glucose medium supplemented with 10% Fetal Bovine Serum (FBS) and 1% penicillin/streptomycin antibiotic) at 37 °C for 24 h. Meanwhile, L929 cells were seeded in 24 well plates (3×10^4 cells per well) and incubated for 24 h before the cytotoxicity test. The culture media of the cells were replaced with the extracts and cells were incubated for a further 24 h. The cell culture treated only media (having no extracts) were used as the control. The number of cells was determined with the Alamar Blue cell proliferation assay.

2.5.2 Isolation and culture of bone marrow mesenchymal stem cells (BMSCs). In the construction of the tissue engineered products *in vitro* and *in vivo*, bone marrow mesenchymal stem cells (BMSCs) isolated from New Zealand white rabbits (6 months old, male) were used. Femurs and tibias were aseptically excised and transferred into penicillin and streptomycin containing MEM-α (1×) + GlutaMAX™ media. The metaphyseal regions of the bones were cut and the marrow in the midshaft was collected in a 50 mL sterile centrifuge tube. The cells were centrifuged at 1700 rpm for 5 min to eliminate fat cells. The resulting cell pellet was resuspended in the primary medium and plated in T-175 flasks. After incubation for 1 week, BMSCs were detached and frozen in FBS containing 10% DMSO and stored in liquid nitrogen until use.

All cell culture experiments were conducted under standard culture conditions in a CO_2 incubator (37 °C, 5% CO_2). Complete media were used for cell seeding and further incubation. Osteogenic media (50 μg mL^{-1} L-ascorbic acid, 10 nM dexamethasone and 10 mM β-glycerophosphate) was used to promote osteoblastic differentiation (phenotype expression) of the bone marrow mesenchymal cells.

2.5.3 Cell adhesion and proliferation assays. Both sides of the cylindrical scaffolds were sterilized under UV for 30 min and then about 50 μL of BMSCs suspension was added. Samples were maintained in a CO_2 incubator for 4 h prior to addition of the medium to ensure cell attachment onto the scaffolds. At the end of the incubation, the volume of the medium in the wells was completed to 1 mL. The number of viable cells on the samples was determined with Alamar Blue assay at predetermined time points (days 1, 7, 14 and 21).

2.5.4 Cell morphology analysis by SEM. The morphology of BMSCs on the scaffolds was examined under SEM (FEI Quanta 400F, The Netherlands) at the end of 21 days of incubation. The cell seeded scaffolds were washed with PBS (10 mM, pH 7.4) twice, fixed with 4% PFA for 30 min at RT, and freeze dried prior to SEM analysis.

2.5.5 Determination of osteogenic differentiation

2.5.5.1 Alizarin red staining. Calcium deposition by BMSCs on the scaffolds was studied by Alizarin red (AR) staining. Cells on the scaffolds were washed with PBS and fixed in 4% paraformaldehyde (PFA), and stained with Alizarin red solution for 15 min at room temperature. The stereomicrographs of the stained scaffolds were obtained.

2.5.5.2 ALP assay. The alkaline phosphatase (ALP) activity of BMSCs was determined using an ALP kit by conversion of *p*-nitrophenyl phosphate to *p*-nitrophenol. Briefly, BMSC

seeded scaffolds were washed with PBS and transferred into lysis buffer. Then, the samples were lyophilized, sonicated (30 s, 25 W) on ice, and centrifuged (2000 rpm, 10 min), and 50 μL of *p*-nitrophenyl phosphate solution was added to 50 μL of the supernatant and incubated (37 °C, 1 h). The absorbance was measured with UV-Vis spectrophotometry at 405 nm. The amount of enzyme was calculated from a calibration curve prepared with known concentrations of *p*-nitrophenol.

2.5.5.3 Quantitative real-time polymerase chain reaction (qRT-PCR). Quantitative Real Time Polymerase Chain Reaction (qRT-PCR) was performed to measure the osteogenic differentiation of BMSCs seeded on scaffolds. Primers were designed for RUNX2, COL1A1, SPP1 and GAPDH genes (Table 1). RUNX2 is a transcriptional factor which plays a role in controlling skeletal development. RUNX2 regulates the differentiation of osteoblasts and the expression of many extracellular matrix protein genes including COL1A1 and SPP1 during osteoblast differentiation.[22] The PCR reaction was as follows: initial denaturation at 95 °C for 10 min, followed by 45 cycles of 95 °C for 10 s, 58 °C for 30 s and 72 °C for 30 s. A cycle threshold (Ct) value was obtained for each sample and averages of duplicate sample values were obtained. Fold changes of each target gene were calculated with the $2^{-\Delta Ct}$ relative quantification method. The mean Ct value of each target gene was normalized to the averaged Ct value of housekeeping gene (GAPDH), which gives the ΔCt value. Finally, fold changes were calculated with the $2^{-\Delta Ct}$ formula.

2.6 *In vivo* studies

In vivo studies were carried out for the scaffolds before bone implantation to check the biocompatibility, and after the implantation to check tissue regeneration.

2.6.1 *In vivo* biocompatibility tests. Biocompatibility tests (intracutaneous irritation and subcutaneous implantation) were performed by 'the Genetic Engineering and Biotechnology Institute' of TUBITAK (The Scientific and Technological Research Council of Turkey) at Marmara Research Center (MAM), which is an organization certified by the 'Ministry of Forestry and Urbanization of Turkey' and analyses performed according to Animal Experiments Ethical Committee Working Principles and Regulations (19.02.2013-313). These tests are explained below.

2.6.1.1 Intracutaneous irritation test. Intracutaneous irritation tests were carried out according to ISO 10993-10: 2010 and ISO 10993-12: 2012 standards. New Zealand albino rabbits (8–12 weeks old) were used for this test. PBS (polar solvent) and corn oil (non-polar solvent) extracts of the scaffolds were administered to the rabbits by intradermal injection. The same solvents were used as controls. Injection sites were examined and scored at 24th, 48th and 72nd h.

2.6.1.2 Subcutaneous implantation test. Implantation tests were carried out according to ISO 10993-6: 2007 and ISO 10993-12: 2012 standards. Implantation tests determine the local effects of biomaterials during implantation and involve macroscopic and microscopic histological examinations. Silicone was used as the control material. Test materials and negative controls were implanted in the lumbodorsal site of Sprague Dawley rats (3–4 months old). Local effects were studied at the end of 28 days by dissecting the implantation and control regions. These regions were fixed with 4% PFA and then dehydrated with increasing concentrations of alcohol series. Dehydrated tissues were embedded in paraffin blocks and 5 μm thick sections were obtained. These sections were then stained with hematoxylin–eosin (H&E) for the histological examination.

2.6.2 Tissue regeneration. Orthotopic implantation tests were carried out at Yeditepe University according to the Animal Experiments Ethical Committee Approval, in agreement with Ministry of Forestry and Urbanization of Turkey Animal Experiments Ethical Committee Working Principles and Regulations (19.02.2013-313).

2.6.2.1 Orthotopic implantation of 3D scaffolds. In these implantation tests, BMSC-seeded and cell-free PCL/HAp and PCL/HAp/PPF scaffolds were applied to New Zealand white rabbits (male, 6–8 months old). BMSC-seeded scaffolds (PCL/HAp and PCL/HAp/PPF) (1×10^6 cells per scaffold) were incubated for 10 days in osteogenic medium before the implantation. Surgeries were performed under anesthesia with ketamine (35 mg kg^{-1}) and xylazine (5 mg kg^{-1}). Defects (diameter 5 mm, height 2.5 mm) were created with a drill on the right femurs of the rabbits, and the samples were introduced into these defects. Antibiotic (Novosef IM Flakon; 100 mg kg^{-1}, Zentiva-Sanofi, France) was administered intramuscularly twice a day for 3 days post-op. The animals were sacrificed at the end of 4 and 8 weeks by inhalation of CO_2.

2.6.2.2 Micro-CT analysis. Computer tomographic assessment was performed to investigate the extent of bone regeneration and healing in terms of regenerated bone volume and

Table 1 Real-time PCR primer details

Gene	Primer nucleotide sequence	Product size (bp)	Genbank accession number
RUNX2	F: GCCACCACCCACTACCATAC R: GCTTCCATCAGCGTCAACAC	258	XM_008262992
COL1A1	F: AGAAATCCGCTGGAGTCTCG R: TCCGTTTTCACCAGGGCTAC	380	XM_008271783
SPP	F: CGTGGTGACAGTGTGGCTTA R: GTGACTTTGGGTTTCCACGC	249	NM_001082194
GAPDH	F: GAAGGTCGGAGTGAACGGAT R: TCTCGCTCCTGGAAGATGGT	231	NM_001082253

bone mineral density (BMD). Hydroxyapatite calibration rods with densities of 0.25 and 0.75 g cm^{-3} were scanned under the same conditions as for the rabbit bones for the calibration of BMD. The samples were scanned using 100 kV and 100 μA power and with 12 μm per pixel. An Al/Cu filter was used to reduce the beam hardening, a 3 frame average was used to reduce the noise, and each frame was obtained in 1710 ms. The samples were rotated 0.4° throughout 360°. Software CTAn and CT Vol Realistic 3D Visualization (Bruker μ-CT, Belgium) were used for image processing in the CT reconstructions and in the creation and visualization of the 3D representations.

2.6.2.3 Biomechanical analysis. Four-point bending tests were performed in order to study the structural integrity of the new bone bridging into the femur defects. The test was performed by using a Mechanical Tester (Shimadzu AGS-X Universal Test Machine, Japan), controlled by a computer running program (Trapezium-X). Scaffold implanted femurs (right femur) were compared with their healthy counterparts (left femur). Rabbit femurs were placed on the same horizontal plane, where the two lower stabilizing points were 45 mm apart and the two upper loading points were 17 mm apart from each other. The test was performed at 5 mm s^{-1} and a maximum load of 200 N was applied. The stiffnesses of the scaffold implanted femurs and their healthy counterparts were calculated.

2.6.2.4 Histological analysis. Following the dissection of the bones, samples were fixed with formalin (10%, pH 7.0) and decalcified with Shandon TBD-2 Decalcifier for 14 days prior to sectioning for histological analysis to study the integration of the bone and the scaffold, tissue response to the implant and bone formation within the defect. The samples were dehydrated in increasing concentrations of alcohol series and embedded in paraffin. Longitudinal sections (5 μm thick) were cut and deparaffinized before staining. Sections were stained with Hematoxylin–Eosin (H&E) and Masson's trichrome and examined under a light microscope.

2.7 Statistics

All experiments were carried out in triplicate. Statistical analyses were performed using GraphPad Prism version 6.0 (GraphPad, San Diego, CA, USA). p-Values ≤ 0.05 were considered significant.

3. Results

3.1 Physical and chemical characterization of 3D scaffolds

PCL based 3D-printed porous scaffolds were prepared by the FDM method. It has been known that the ultimate success of the implants in tissue regeneration is influenced by design parameters such as pore size, porosity, interconnectivity of pores, pore size distribution within the scaffold, surface chemistry and mechanical properties.[23,24] In this study, the scaffold architecture was modified by changing the respective position of the deposited fibers. The scaffolds were examined under a stereomicroscope, SEM and μ-CT (Fig. 1). It is seen that pore sizes and fiber dimensions did not change significantly when different shift distances were used since the printing parameters (such as extrusion temperature and printing rate in the x and y directions) were kept constant. The pore size of the scaffolds was found to be around 350 μm. In the literature, it is stated that scaffolds with a pore size in the range 100–500 μm lead to osteoconductivity.[25,26] Porosities of the different scaffolds were found to increase from 26 to 35% as the shift distance decreased. The lower porosity of the basic shift (BS) scaffolds might be due to flattening of the shifted fibers since they could not be supported with the fibers of the underlying layers. Based on the collective results of the SEM, micro-CT and porosity analysis, B0 and BS0.10 scaffolds were found to have a higher porosity and a more open pore structure compared to other BS scaffolds. This led to the leakage of the cells during cell seeding and the resultant poor cell adhesion numbers. On the other hand, BS0.20, BS0.25 and BS0.50 have a less open pore structure, which may lead to insufficient cell infiltration and bone ingrowth. Therefore, BS0.15 PCL scaffolds were chosen for use in the following investigations since they have moderate porosity to support cell attachment (*in vitro*) and bone ingrowth (*in vivo*) due to the interconnected open pores in their structures.

PCL/HAp and PCL/HAp/PPF composite scaffolds were prepared by coating the PCL scaffolds with HAp and with HAp/PPF. The morphology, porosity and distribution of HAp over the composite scaffolds were analyzed with SEM, micro-CT and EDS analysis (Fig. 2A–J). It was found that coating with HAp and PPF did not significantly affect the porosity of the composite scaffolds (PCL: 31 ± 4%, PCL/HAp: 35 ± 3% and PCL/HAp/PPF: 36 ± 3%). As can be seen in the micro-CT images, HAp particles were distributed homogenously over the fibers throughout the PCL/HAp and PCL/HAp/PPF scaffolds. Moreover, the presence of HAp particles on the scaffolds was confirmed by EDS analysis (Fig. 2J). The weight percent of Ca and P elements on PCL/HAp scaffolds (Ca: 6.53% and P: 4.52%) was higher than that of the PCL/HAp/PPF scaffolds (Ca: 1.22% and P: 0.76%) most probably because the PPF matrix covered and masked the detection of HAp particles.

The wetting behavior of the scaffolds was investigated by measurement of the water contact angle (WCA) (Fig. 2K). For PCL and PCL/HAp scaffolds, the drop was stable on the samples for 5 s, while for PCL/HAp/PPF, a quick decrease in WCA indicates a hydrophilic surface. It is stated in the literature that a moderately hydrophilic surface leads to a higher cell attachment compared to a hydrophobic surface.[27–29] Pristine PCL scaffolds had a WCA of 80° while PCL/HAp had a lower WCA value of 65°. Introduction of hydroxyapatite particles onto the fibers increased the hydrophilicity of PCL due to the ionic nature of HAp. PPF containing scaffolds had an even lower water contact angle value (50° at the first second but immediately decreased to 32° in 5 s). PPF is known to be a hydrophobic polymer. It was reported that the WCA of cross-linked PPF was 69° and decreased to 35° upon incorporation of HAp.[30] In our experiments, similar hydrophilicity was obtained for the PCL scaffolds coated with HAp and HAp/PPF.

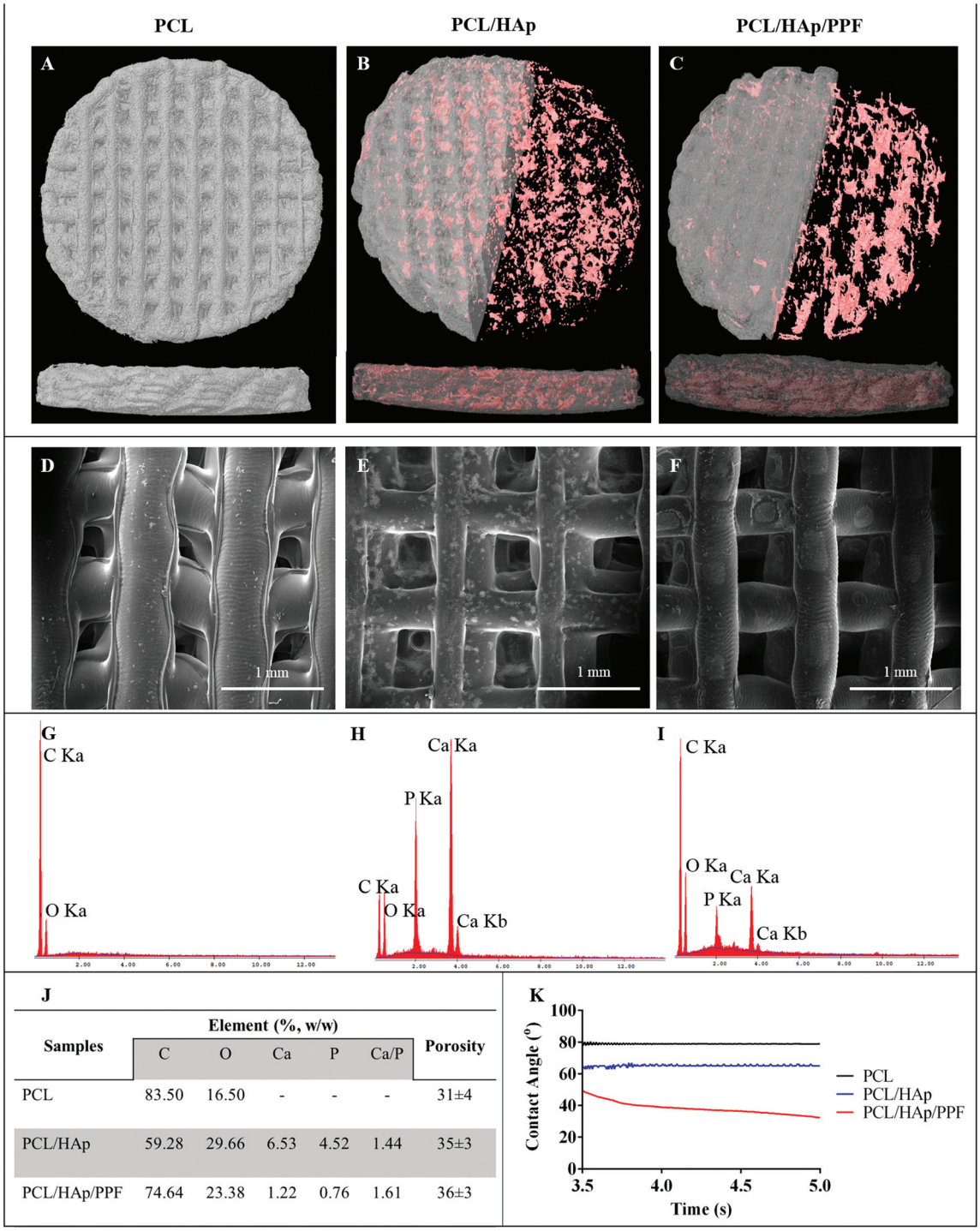

Samples	Element (%, w/w) C	O	Ca	P	Ca/P	Porosity
PCL	83.50	16.50	-	-	-	31±4
PCL/HAp	59.28	29.66	6.53	4.52	1.44	35±3
PCL/HAp/PPF	74.64	23.38	1.22	0.76	1.61	36±3

Fig. 2 Physical and chemical characterization of the PCL, PCL/HAp and PCL/HAp/PPF scaffolds designed in the BS0.15 form. (A–C) Micro-CT results (top view) and the distribution of the HAp particles in the scaffolds (red). The cross-section in the *z*-direction shows the distribution of the HAp over the fibers. (D–F) SEM micrographs of the scaffolds. (G–I) EDS results showing the presence of Ca and P ions. (J) EDS analysis of C, O, Ca and P elements and porosity values. (K) Water contact angles of the scaffolds (PCL: A, D, G; PCL/HAp: B, E, H; PCL/HAp/PPF: C, F, I).

3.2 Mechanical analysis

Electromagnetic radiation is commonly used for the sterilization of tissue grafts before implantation. It has been reported that irradiation with high energy gamma rays may lead to the formation of reactive intermediates on polymers and these intermediates are involved in several reaction pathways, which may cause crosslinking or scission of the polymer backbone or

the side chains.[31,32] These reactions affect the mechanical properties of the polymers.[33] In order to study the effect of the gamma irradiation on the mechanical properties of the scaffolds, compression tests were performed before and after gamma irradiation and stress–strain curves were plotted (Fig. 3A). As can be seen in the figure, gamma irradiation did not significantly affect the mechanical properties of the scaffolds.

It is possible to tune the mechanical properties that would match with the mechanical requirements of different tissues, through the adjustment of the fiber positioning within the scaffold architecture.[34,35] In this study, the effect of the scaffold design and chemical composition on the mechanical properties of the scaffolds was investigated with a compression test (Fig. 3B). The compressive modulus was found to decrease from 37.52 ± 0.50 to 22.80 ± 1.29 MPa upon the change in fiber organization of the PCL scaffold from basic (B) to basic shift (BS0.15) architecture (Fig. 3B). The lower compressive modulus of the BS scaffold is likely to be attributable to the shifted fibers where the fibers of subsequent layers do not support each other.[36]

Compressive modulus did not change significantly by addition of HAp as a coat onto the BS PCL scaffold. Meanwhile, the HAp/PPF coat increased this value from 22.80 ± 1.29 MPa to 33.74 ± 1.08 MPa. In the literature, it is stated that PPF-based composite materials have a compressive modulus in the range 23–265 MPa[37,38] and is suitable to replace the human trabecular bone which has a compressive elastic modulus of 50–100 MPa.[39] It was proposed that this large change in PPF properties could arise from differences in the molecular weight and crosslinking density of PPF.[40] So that, it is possible to further improve the mechanical properties of PPF based scaffolds by changing the chemical properties and the architecture of PPF scaffolds.

3.3 Evaluation of *in situ* degradation

Scaffolds used in tissue engineering applications are designed to degrade at a degradation rate suitable for removal in a reasonable period while supporting the tissue that is undergoing regeneration. Information about the degradation rates of scaffolds is therefore very important. The enzymatic degradation profiles of 3D printed scaffolds under *in situ* conditions were investigated in aqueous solutions of lipase, an enzyme secreted by the macrophages.[41] Chemistry, morphology, and porosity are the main factors that affect the degradation rate of the scaffolds the most. Hydrolytic enzymes such as lipase enzyme are adsorbed onto the polymer surface before initiating hydrolysis.[42] Lipase enzyme cleaves the ester bonds of PCL because of its structural similarity to lipids.[43] Fig. 3C shows the weight loss profiles of the PCL based on lipase. Incorporation of HAp onto the scaffold increased its degradation rate. It has been shown earlier that the incorporation of a bioceramic like HAp into polymers increases polymer degradation, because the ceramic fillers act as "defects" and enhance water absorption, increasing the rate of media diffusion into the coat and also increase the surface area for hydrolytic attack. Thus, HAp incorporation enhances the surface hydrophilicity and increases the invasion of the enzyme and water into the scaffolds.[44] The PCL/HAp/PPF scaffolds demonstrated the highest degradation rate among the three sample types because of the additional increase in

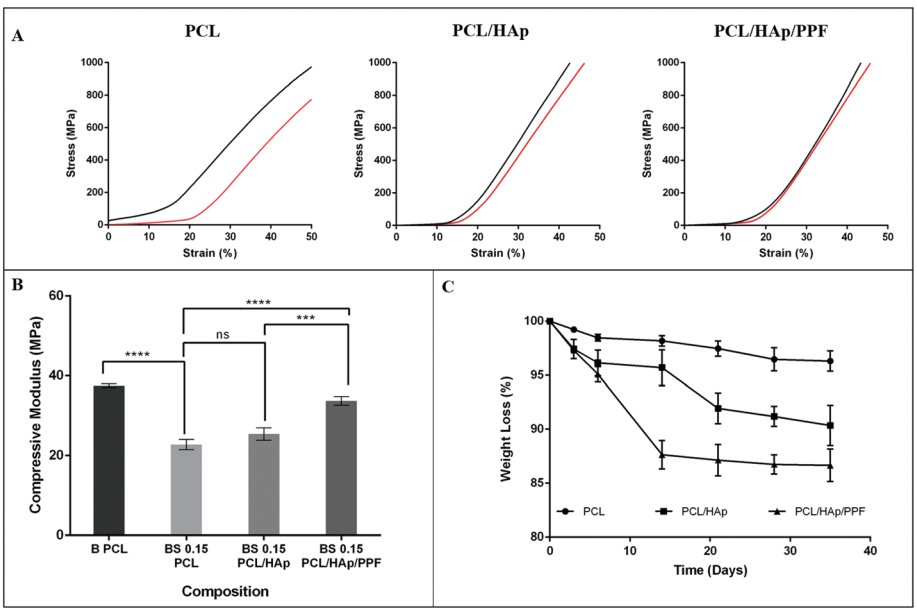

Fig. 3 (A) Stress–strain curves of PCL, PCL/HAp and PCL/HAp/PPF scaffolds before and after gamma irradiation (black: before, red: after irradiation). (B) Compressive modulus of PCL (B and BS0.15), and BS scaffolds of PCL/HAp and PCL/HAp/PPF. (C) Weight loss of BS scaffolds of PCL, PCL/HAp and PCL/HAp/PPF in aqueous lipase solution (180 U L^{-1}) in 35 days. Statistical analysis was carried out by using one-way ANOVA. *p < 0.05, **p < 0.01, ***p < 0.005, ****p < 0.0001, and ns: not significant.

hydrophilicity as mentioned previously, as shown by a decrease in water contact angle values.

3.4 *In vitro* studies

3.4.1 Cytotoxicity of 3D scaffolds. The cytotoxicity test was conducted on the L929 fibroblasts using the complete media extracts of the scaffolds which were prepared by incubation of the scaffolds in the media in accordance with the ISO 10993-5 standard test method. Cell viability was measured with Alamar Blue cell proliferation assay. Fig. 4A shows the number of cells which were cultured with the extraction media in comparison with those cultured with complete media as a control. PCL and HAp have earlier been used in bone tissue engineering without any cytotoxic effect.[45] However, it was shown that uncrosslinked PPF copolymers are highly cytotoxic (viability <3%) compared with cross-linked networks (viability >80%).[46] The results presented in Fig. 4(A and D) suggest that all the scaffolds were nontoxic, and none of the extracts presented any risk of cytotoxicity.

3.4.2 BMSC proliferation on 3D scaffolds. Cell viability was evaluated based on the number of viable cells that adhered to and proliferated on the scaffolds at days 1, 7, 14 and 21 using Alamar Blue assay. PCL scaffolds (B and BS0.15) were compared in terms of cell attachment efficiency and viability (Fig. 4B and E). Cell adhesion was significantly higher in the BS PCL scaffolds than in the B PCL, probably because of the larger contact area between the cells and the scaffold in the BS construct, and also the path of the media flow through the scaffold. In earlier studies carried out by our group we observed similar results[35] while similar results were also reported by Yeo *et al.*[25] In the case of the basic structure, cells have a clear open path along the height of the cylinder and

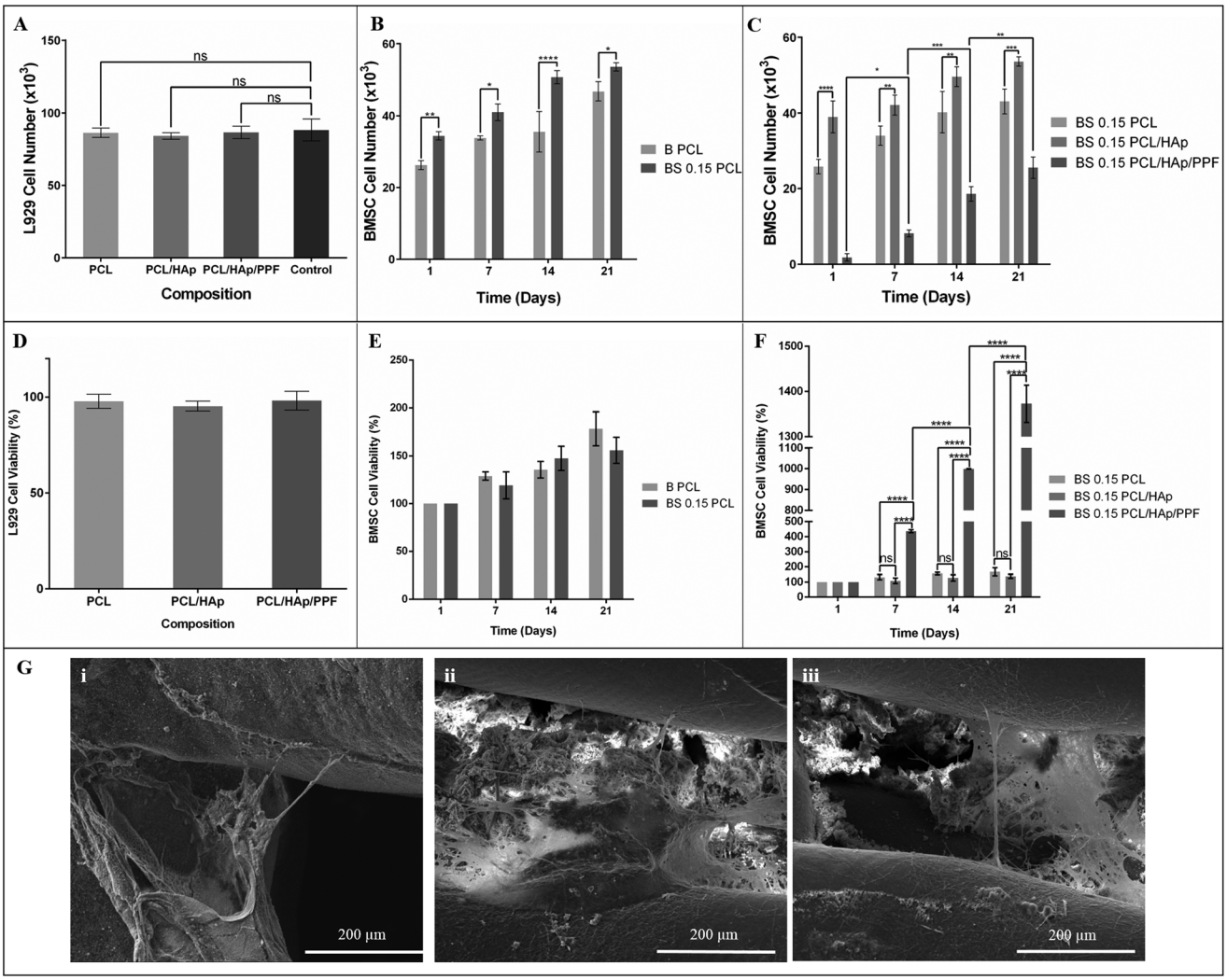

Fig. 4 (A and D) Cytotoxicity of PCL, PCL/HAp and PCL/HAp/PPF scaffolds performed on fibroblasts (L929) in accordance with ISO 10993-5 using the extracts after incubation of the scaffolds in the complete medium at 37 °C for 24 h. (B and E) Viability of BMSC on PCL scaffolds (B and BS0.15) at 21 days as studied by the Alamar Blue cell viability test. (C and F) Viability of BMSC on the BS scaffolds of PCL, PCL/HAp and PCL/HAp/PPF. (G) SEM micrographs of BMSC seeded scaffolds (i) PCL, (ii) PCL/HAp, and (iii) PCL/HAp/PPF (day 21). Statistical analysis was carried out by using one-way ANOVA and two-way ANOVA. *$p < 0.05$, **$p < 0.01$, ***$p < 0.005$, ****$p < 0.0001$, and ns: not significant.

passed and leaked through these channels in the scaffold. However, cells found higher chance of contact in BS0.15 PCL scaffolds due to tortuous pathways of flow in these scaffolds, which leads to improved initial adhesion and subsequent higher cell numbers. Therefore, BS0.15 scaffolds were chosen for the later *in vitro* and *in vivo* experiments.

The effect of the surface chemistry of the scaffold on BMSC viability was also evaluated (Fig. 4C and F). For PCL/HAp scaffolds higher adhesion and higher cell numbers during the whole test duration were observed. The presence of HAp nanoparticles which is reported to be osteoconductive provided better support for cell adhesion and proliferation. It is also suggested that HAp particles may facilitate adsorption of specific serum proteins that could help and regulate the adhesion and proliferation of the cells.[47] The presence of PPF in the scaffold coat composition, however, adversely affected the initial attachment of the cells. This is partly because of the increased hydrophilicity of the PCL/HAp/PPF scaffolds as mentioned previously as shown by a decrease in water contact angle values. It has been reported that material surfaces should have moderate wettability with water contact angles of 40°–70° for optimal cell adhesion.[48,49] The number of cells

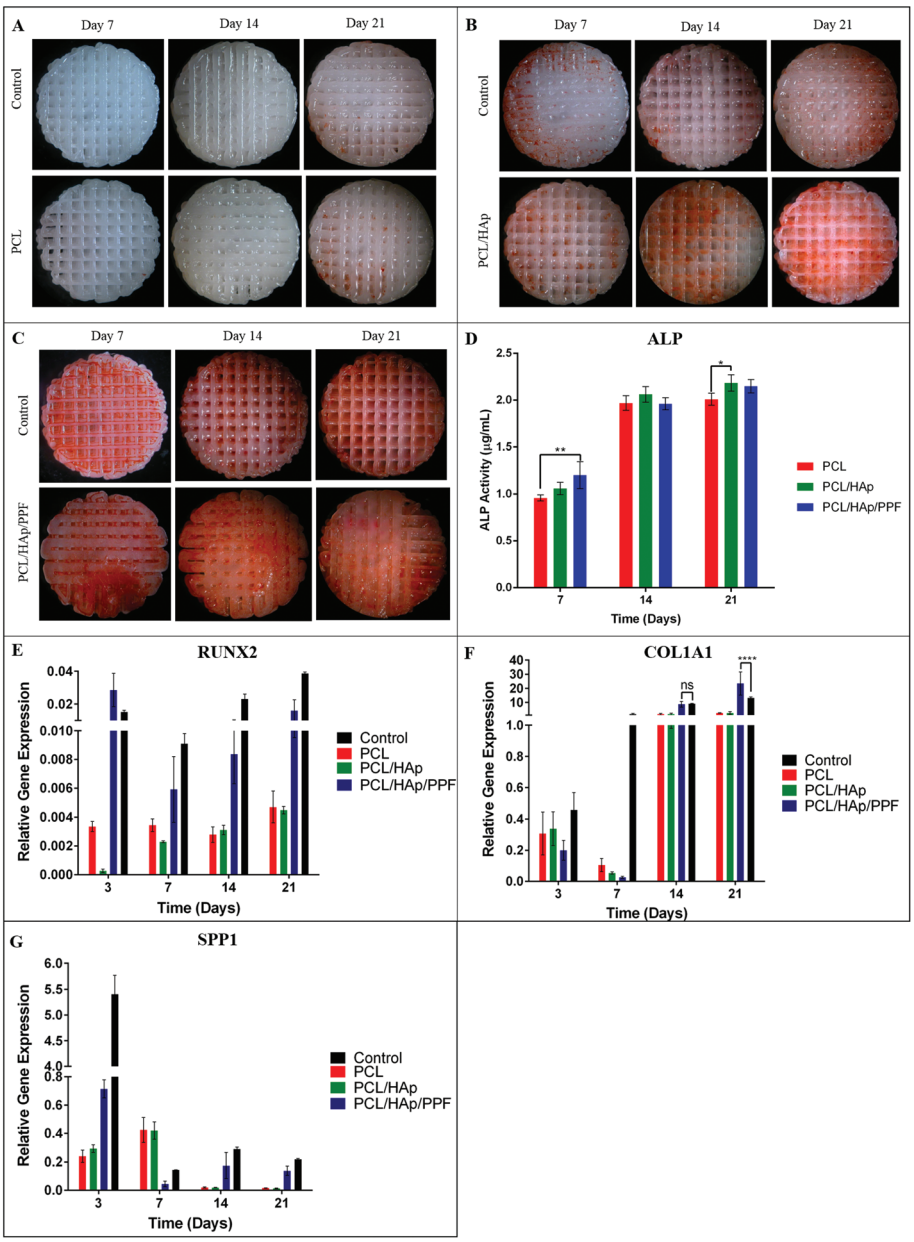

Fig. 5 Osteogenic differentiation of the BMSCs on the PCL, PCL/HAp and PCL/HAp/PPF scaffolds (all scaffolds are BS). (A–C) Light microscope images of the AR staining on days 7, 14 and 21. (D) ALP activities on days 7, 14 and 21. Quantitative RT-PCR results on days 7, 14 and 21 for (E) RUNX2, (F) COL1A1 and (G) SPP1 genes. Statistical analysis was carried out by using two-way ANOVA. *$p < 0.05$, **$p < 0.01$, ***$p < 0.005$, ****$p < 0.0001$, and ns: not significant.

that adhered to the surface of PCL/HAp/PPF scaffolds was much less than that on PCL and PCL/HAp scaffolds, however, the cell proliferation rate was much higher than that on the others. The number of cells increased by almost 14 fold on PCL/HAp/PPF scaffolds while the increase was less than 2 fold on PCL and PCL/HAp scaffolds (Fig. 4F).

3.4.3 Morphological analysis of BMSCs on 3D scaffolds by SEM. The cellular morphology of the BMSCs seeded on PCL, PCL/HAp and PCL/HAp/PPF scaffolds was investigated on day 21 of the cell culture using SEM (Fig. 4G). The results indicated that the cells attached and spread well on all scaffolds; the cells did not only spread on the fibers, but they also spread across the fibers and attempted to fill the pores of the scaffolds with secreted ECM. These indicate that the substrate surface properties are very suitable for BMSC adhesion regardless of surface chemistry.

3.4.4 Osteogenic differentiation

3.4.4.1 Alizarin red staining. Upon differentiation BMSCs enter into the mineralization phase and deposit mineralized ECM. The capacity of BMSCs to deposit minerals is a marker for osteogenic efficiency and was monitored by Alizarin red (AR) staining of the calcium phosphate minerals on the scaffolds on days 7, 14 and 21. Fig. 5A–C show the light microscope images of BMSC seeded scaffolds and cell free (control) scaffolds stained with AR where red color indicates the calcium phosphate crystals.

The calcium deposition on the PCL/HAp and PCL/HAp/PPF scaffolds was higher than that of the pure PCL scaffold, and the color intensity increased over 21 days, suggesting that the amount of calcium phosphate on the scaffolds increased. This observation is in accordance with the study of Chuenjitkuntaworn *et al.* (2010)[50] in which positive staining for calcium deposition was observed with increasing HAp concentration in the electrospun PLLA/HAp scaffolds.

3.4.4.2 ALP assay. Alkaline phosphatase enzyme (ALP) is an early indicator of immature osteoblast activity, which plays a significant role in the formation of bone mineral and shows the commitment of the stem cells towards the osteoblastic phenotype.[51] The ability of the PCL based scaffolds to promote osteogenic differentiation was studied by measuring the ALP activity on days 7, 14 and 21 (Fig. 5D). There was a significant increase in the ALP activity between days 7 and 14 for all scaffolds. By day 21, the ALP activity of all the scaffolds reached a plateau. The ALP activity of the HAp containing scaffolds was higher than the PCL scaffold especially on day 7 and 21, which is due to the osteogenic feature of the HAp.[52]

3.4.4.3 Quantitative real-time polymerase chain reaction (RT-PCR). Quantitative RT-PCR analysis was performed as a molecular approach in addition to ALP production and the genes RUNX2, COL1A1 and SPP1 were studied to investigate the osteogenic differentiation of BMSCs on the scaffolds. The RUNX2 gene plays an important role in the production and regulation of bone matrix proteins. In this study it was found that the RUNX2 expression on PCL/HAp/PPF scaffolds was significantly higher than on the PCL and PCL/HAp scaffolds (Fig. 5E). COL1A1 is the gene responsible for the production of a certain section of collagen Type 1, the most abundant protein in the bone matrix. The highest COL1A1 expression was observed on days 14 and 21 for the scaffolds and the control group (Fig. 5F). However, BMSCs expressed COL1A1 on the PCL/HAp/PPF scaffold higher than on the control group on day 21. SPP1 expression was also investigated (Fig. 5G). During bone repair SPP1 plays an important role in the clearance of debris by macrophage phagocytosis and the formation of new bone at the edges of the bone defects. It was found that the SPP1 expressions for the PCL/HAp/PPF and control groups were higher than for the other groups with the control's being the highest, on days 3, 14 and 21. In addition, there were no significant differences between these two groups on days 14 and 21.

3.5 *In vivo* studies

3.5.1 *In vivo* biocompatibility tests

3.5.1.1 Intracutaneous irritation test. Various immune cells that are responsible for both innate and acquired immunity are distributed in the skin and when the skin comes in contact with harmful substances, irritation occurs, with symptoms like erythema and edema.[53] In accordance with the ISO 10993-10 which defines the approach for *in vivo* biocompatibility, intracutaneous irritation tests were performed using PCL, PCL/HAp and PCL/HAp/PPF scaffolds. The scores were determined as 0.13, 0.11 and 0.20 (ESI 2a†), indicating levels of negligible irritation caused by the scaffolds on the skin of New Zealand albino rabbits. In the literature it is reported that extracts of PCL, HAp and PPF were studied individually for causing skin irritation and it was found that none of them led to irritation.[54–56]

3.5.1.2 Subcutaneous Implantation test. Even though PCL is an FDA approved biocompatible polymer for use in humans, composite PCL scaffolds had to be evaluated to determine whether they had any local effects when implanted subcutaneously. The 3 scaffolds were implanted subcutaneously in rats and the implantation sites were observed after 28 days. The scores

Fig. 6 Implantation of scaffold into the femur of a New Zealand rabbit.

based on number and type of inflammatory cells indicate that the PCL, PCL/HAp and PCL/HAp/PPF scaffolds induced no inflammatory response; all the severity scores were lower than the lowest limit 2.9 (ESI 2b†). In the study by Ghanaati *et al.* (2012)[57] HAp granules were implanted subcutaneously into rats, and the early and late inflammatory responses were followed for 30 days at four time points. The histological and histomorphometrical analyses revealed that HAp in granulated form leads to low levels of early and late inflammation. According to a study of Fisher *et al.* (2002),[58] implanted PPF was studied for 8 weeks both histologically and histomorphometrically. It was reported that the PPF scaffolds led to

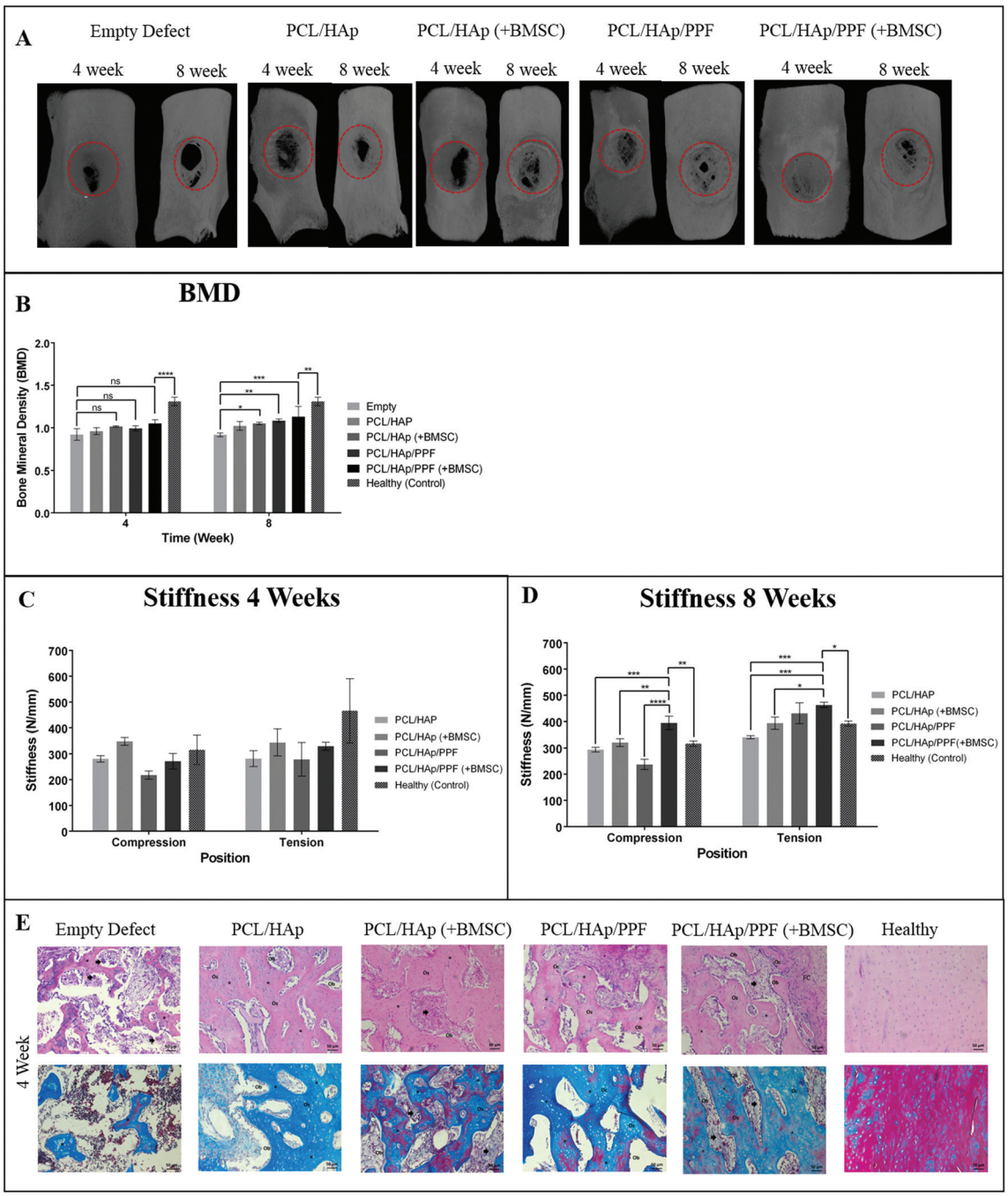

Fig. 7 Evaluation of *in vivo* bone tissue regeneration. (A) Micro-CT images (dotted red circles show the defect site), (B) bone mineral density values, (C) stiffness values at the position of compression and tension at 4 weeks and (D) 8 weeks, (E) histological photomicrographs of the BMSC seeded and unseeded PCL/HAp and PCL/HAp/PPF scaffolds (both BS0.15) after 4 weeks of implantation. (* denotes new bone formations, arrows indicate foreign body giant cells and macrophages, FC: fibrous connective tissue, Ob: osteoblasts, Os: osteocytes, Oc: osteoclasts.) Statistical analysis of BMD results was carried out by using two-way ANOVA. *$p < 0.05$, **$p < 0.01$, ***$p < 0.005$, ****$p < 0.0001$, and ns: not significant.

minimal fibrous encapsulation and PPF was categorized as biocompatible within both soft and hard tissue.

3.5.2 Evaluation of *in vivo* bone tissue regeneration

3.5.2.1 Micro-CT analysis. In order to investigate the osteoinductive and osteoconductive potential of the 3D scaffolds, unseeded and BMSC seeded PCL/HAp and PCL/HAp/PPF scaffolds were implanted orthotopically in the femoral defects of the New Zealand white rabbits (Fig. 6). Micro-CT was used to quantitatively analyze the extent of new tissue formation and bone mineral density (BMD). It is seen that, after 8 weeks, the control (untreated empty defect) recovered at a minimum level with regions of very low mineralization at the edges of the defect. Regions with moderate mineralization were detected in the defects into which BMSC free PCL/HAp scaffolds were placed. These scaffolds displayed better closure with bone formation from the edges towards the center of the defect. However, the scaffolds containing BMSCs demonstrated greater healing in all cases (Fig. 7A). The bone mineral densities of the defects into which scaffolds were implanted were significantly higher than that of the control (untreated empty defect) (Fig. 7B). After 8 weeks of implantation, it was also observed that the defects with BMSC seeded PCL/HAp/PPF scaffolds mineralized at very high levels, comparable to the BMD values of the healthy bone.

3.5.2.2 Biomechanical analysis. The four point bending test was applied to femurs after 4 and 8 weeks of implantation to evaluate the healing of the bones in terms of biomechanical performance. The stiffness of the implanted femurs was tested at compression and tension positions. The stiffness increased for all groups from 4 to 8 weeks, which indicates that the defects were healing (Fig. 7C and D). The stiffness of the defects treated with BMSC seeded scaffolds demonstrated a significant increase compared to cell free scaffolds at both 4 and 8 weeks, which suggests that the presence of the cells enhanced the healing of the defect. Although both the BMSC seeded and BMSC free PCL/HAp scaffolds led to better biomechanical properties at week 4, PCL/HAp/PPF implanted femurs displayed better stiffness at the end of the test duration (8 weeks). After 8 weeks of implantation, BMSC seeded PCL/HAp/PPF scaffolds in particular, displayed a significantly higher stiffness when tested at both compression and tension positions. Based on Fig. 7D data, it can be concluded that after 8 weeks of implantation, the BMSC seeded PCL/HAp/PPF scaffold implanted femurs recovered more successfully than the other scaffolds.

3.5.2.3 Histological analysis. A histological study was performed in order to obtain more information about the repair process at the cellular level. Histological micrographs of tissue sections through the femoral bone defects at 4 weeks post-op are presented in Fig. 7E following H&E, and Masson's trichrome staining.

In the control (empty defect) extensive fibrous connective tissue and small amounts of new bone formation are seen in the form of spicule and trabecula. Also, intense bleeding sites in the gaps between the trabecula and a significant amount of foreign body giant cells and macrophages were observed. In contrast, when scaffolds were implanted at the defect site low levels of fibrous connective tissue formation and less bleeding were observed. Besides, thicker trabecula formed and new bone tissue formation occurred by the fusion of these trabecula. In all the experimental groups, osteoblasts which are the precursor cells involved in the new bone formation and osteocytes, the mature bone cells, were detected. Additionally, osteoclasts, which play a huge role in bone removal and remodeling, were present at the surface of trabecula. When the scaffold groups were compared, it can be concluded that there was no significant difference between the PCL/HAp and PCL/HAp/PPF implanted defects. However, there was more intense connective tissue formation in the defects into which BMSC seeded scaffolds were implanted. Shao *et al.* investigated the *in vivo* the effect of PCL based scaffolds with or without BMSCs. It was reported that scaffolds with BMSC led to better osteochondral tissue formation compared to the control group which showed limited osteochondral regeneration.[59] Xie *et al.* prepared mesenchymal stem cell derived microvesicles (MSC-MVs) to be incorporated into alginate-PCL scaffolds in order to promote angiogenesis and bone regeneration. Histological analysis showed that more new bone formation was observed in the presence of MV than in their absence.[60]

4. Conclusion

In the present study, PCL scaffolds were printed by the FDM technique having either basic or basic shift geometry, and were modified by coating with HAp and HAp/PPF to produce composite scaffolds. The *in vitro* osteogenic potentials and *in vivo* regenerative capacities of the scaffolds were investigated. Morphological analysis and surface chemical characterization confirmed the homogenous distribution of the HAp particles throughout the composite coats of the scaffolds. Incorporation of HAp/PPF onto the PCL scaffold significantly enhanced the compressive modulus. Biological studies after seeding with BMSCs showed enhanced cell adhesion for PCL/HAp scaffolds, and the proliferation rate of the cells was higher in PCL/HAp/PPF compared to that in the others. Both *in vitro* and *in vivo* biocompatibility tests revealed that the scaffolds did not show any cytotoxicity, irritation and inflammation. Micro-computed tomography images and BMD analysis indicated that the BMSC seeded PCL/HAp/PPF scaffolds had greater tissue regeneration at the end of 8 weeks and their stiffness was very close to that of the healthy bone tissue. Histology revealed a favorable tissue response for all of the scaffold compositions. The results demonstrate that PCL/HAp and PCL/HAp/PPF composite scaffolds hold great promise as regenerative materials for use in bone tissue engineering applications.

Conflicts of interest

There are no conflicts to declare.

Acknowledgements

The authors acknowledge the financial support for this work from TUBITAK (project no 213M708), METU (BAP 07-02-2014-007-348) and BIOMATEN, METU Center of Excellence in Biomaterials and Tissue Engineering. Görkem Cemali (Yeditepe University) is also acknowledged for her support during PPF synthesis. Authors thank Central Laboratory of METU for the SEM analyses.

References

1 R. Burge, B. Dawson-Hughes, D. H. Solomon, J. B. Wong, A. King and A. Tosteson, *J. Bone Miner. Res.*, 2007, **22**(3), 465–475.
2 A. Sutradhar, G. H. Paulino, M. J. Miller and T. H. Nguyen, *Proc. Natl. Acad. Sci. U. S. A.*, 2010, **107**(30), 13222–13227.
3 S. Bhumiratana, J. C. Bernhard, D. M. Alfi, K. Yeager, R. E. Eton, J. Bova, F. Shah, J. M. Gimble, M. J. Lopez, S. B. Eisig and G. Vunjak-Novakovic, *Sci. Transl. Med.*, 2016, **8**(343), 343–383.
4 K. F. Leong, C. M. Cheah and C. K. Chua, *Biomaterials*, 2003, **24**(13), 2363–2378.
5 H. Zhang, X. Mao, Z. Du, W. Jiang, X. Han, D. Zhao, D. Han and Q. Li, *Sci. Technol. Adv. Mater.*, 2016, **17**(1), 136–148.
6 A. Rai, S. Senapati, S. K. Saraf and P. Maiti, *J. Mater. Chem. B*, 2016, **4**, 5151–5160.
7 S. Chen, L. Zheng, X. Xie, X. Wang, Y. Lai, S. Chen, M. Zhang, Y. Wang, J. F. Griffith and L. Qin, *J. Orthop. Translat.*, 2014, **2**(2), 91–104.
8 H. Qi, Z. Ye, H. Ren, N. Chen, Q. Zeng, X. Wu and T. Lu, *Life Sci.*, 2016, **148**, 139–144.
9 M. Abedalwafa, F. Wang, L. Wang and C. Li, *Rev. Adv. Mater. Sci.*, 2013, **34**, 123–140.
10 M. Alhijjaj, P. Belton and S. Qi, *Eur. J. Pharm. Biopharm.*, 2016, **108**, 111–125.
11 E. Nyberg, A. Rindone, A. Dorafshar and W. L. Grayson, *Tissue Eng., Part A*, 2017, **23**(11–12), 503–514.
12 R. Trombetta, J. A. Inzana, E. M. Schwarz, S. L. Kates and H. A. Awad, *Ann. Biomed. Eng.*, 2017, **45**(1), 23–44.
13 J. P. Gleeson, N. A. Plunkett and F. J. Obrien, *Eur. Cells Mater.*, 2010, **20**, 218–230.
14 R. J. Kane, H. E. W. Bilka, M. J. Meagher, Y. Liu, J. A. Gargac, G. L. Niebur, D. R. Wagner and R. K. Roeder, *Acta Biomater.*, 2015, **17**, 16–25.
15 T. Wang, X. Yang, X. Qi and C. Jiang, *J. Transl. Med.*, 2015, **13**(1), 1.
16 D. H. Kempen, L. Lu, C. Kim, X. Zhu, W. J. Dhert, B. L. Currier and M. J. Yaszemski, *J. Biomed. Mater. Res., Part A*, 2006, **77**(1), 103–111.
17 F. K. Kasper, K. Tanahashi, J. P. Fisher and A. G. Mikos, *Nat. Protoc.*, 2009, **4**(4), 518–525.
18 K. Kim, D. Dean, A. G. Mikos and J. P. Fisher, *Biomacromolecules*, 2009, **10**(7), 1810–1817.
19 R. K. Das, S. K. Brar and M. Verma, *Pharmacol. Rep.*, 2016, **68**(2), 404–414.
20 P. X. Lan, J. W. Lee, Y. J. Seol and D. W. Cho, *J. Mater. Sci.: Mater. Med.*, 2009, **20**(1), 271–279.
21 A. M. Martins, Q. P. Pham, P. B. Malafaya, R. A. Sousa, M. E. Gomes, R. M. Raphael, F. K. Kasper, R. L. Reis and A. G. Mikos, *Tissue Eng., Part A*, 2008, **15**(2), 295–305.
22 T. Komori, *Cell Tissue Res.*, 2010, **339**(1), 189–195.
23 S. Bose, M. Roy and A. Bandyopadhyay, *Trends Biotechnol.*, 2012, **30**(10), 546–554.
24 K. Kim, A. Yeatts, D. Dean and J. Fisher, *Tissue Eng., Part B*, 2010, **16**(5), 523–539.
25 M. Yeo, C. G. Simon and G. Kim, *J. Mater. Chem.*, 2012, **22**(40), 21636–21646.
26 B. D. Boyan, T. W. Hummert, D. D. Dean and Z. Schwartz, *Biomaterials*, 1996, **17**, 137–146.
27 A. M. Diez-Pacual and A. L. Diez-Vicente, *ACS Appl. Mater. Interfaces*, 2016, **8**(28), 17902–17914.
28 M. M. Bornstein, P. Valderrama, A. A. Jones, T. G. Wilson, R. Seibl and D. L. Cochran, *Clin. Oral Implants Res.*, 2008, **19**, 233–241.
29 C. Ozcan, P. Zorlutuna, V. Hasirci and N. Hasirci, *Macromol. Symp.*, 2008, **269**, 128–137.
30 K. W. Lee, S. Wang, M. J. Yaszemski and L. Lu, *Biomaterials*, 2008, **29**(19), 2839–2848.
31 R. A. Khan, S. Beck, D. Dussault, S. Salmieri, J. Bouchard and M. Lacroix, *J. Appl. Polym. Sci.*, 2013, **129**(5), 3038–3046.
32 Y. H. A. Fawzy, A. E. H. Ali, G. F. El-Maghraby and R. M. Radwan, *World J. Condens. Matter Phys.*, 2011, **1**, 12–18.
33 J. C. M. Suarez and E. B. Mano, *Polym. Degrad. Stab.*, 2001, **72**(2), 217–221.
34 S. J. Hollister, *Nat. Mater.*, 2005, **4**(7), 518–524.
35 P. Yilgor, R. A. Sousa, R. L. Reis, N. Hasirci and V. Hasirci, *Macromol. Symp.*, 2008, **269**(1), 92–99.
36 S. A. Park, S. H. Lee and W. D. Kim, *Bioprocess Biosyst. Eng.*, 2011, **34**(4), 505–513.
37 J. Yan, J. Li, M. B. Runge, M. Dadsetan, Q. Chen, L. Lu and M. J. Yaszemski, *J. Biomater. Sci., Polym. Ed.*, 2011, **22**(4–6), 489–504.
38 S. J. Peter, S. T. Miller, G. Zhu, A. W. Yasko and A. G. Mikos, *J. Biomed. Mater. Res.*, 1998, **41**(1), 1–7.
39 K. A. Athanasiou, C. F. Zhu, D. R. Lanctot, C. M. Agrawal and X. Wang, *Tissue Eng.*, 2000, **6**(4), 361–381.
40 J. P. Fisher, J. W. Vehof, D. Dean, J. P. van der Waerden, T. A. Holland, A. G. Mikos and J. A. Jansen, *J. Biomed. Mater. Res.*, 2002, **59**(3), 547–556.
41 H. Seyednejad, D. Gawlitta, R. V. Kuiper, A. de Bruin, C. F. van Nostrum, T. Vermonden, W. J. A. Dhert and W. E. Hennink, *Biomaterials*, 2012, **33**(17), 4309–4318.
42 J. Zeng, X. Chen, Q. Liang, X. Xu and X. Jing, *Macromol. Biosci.*, 2004, **4**(12), 1118–1125.
43 M. Mochizuki and M. Hirami, *Polym. Adv. Technol.*, 1997, **8**(4), 203–209.
44 Y. Ito, H. Hasuda, M. Kamitakahara, C. Ohtsuki, M. Tanihara, I. K. Kang and O. H. Kwon, *J. Biosci. Bioeng.*, 2005, **100**(1), 43–49.

45 C. H. Lee, J. Hajibandeh, T. Suzuki, A. Fan, P. Shang and J. J. Mao, *Tissue Eng., Part A*, 2014, **20**(7–8), 1342–1351.
46 M. D. Timmer, H. Shin, R. A. Horch, C. G. Ambrose and A. G. Mikos, *Biomacromolecules*, 2003, **4**(4), 1026–1033.
47 B. Chuenjitkuntaworn, W. Inrung, D. Damrongsri, K. Mekaapiruk, P. Supaphol and P. Pavasant, *J. Biomed. Mater. Res., Part A*, 2010, **94**(1), 241–251.
48 S. M. Oliveira, N. M. Alves and J. F. Mano, *J. Adhes. Sci. Technol.*, 2014, **28**(8–9), 843–863.
49 C. Ozcan and N. Hasirci, *J. Biomater. Sci., Polym. Ed.*, 2007, **18**(6), 759–773.
50 B. Chuenjitkuntaworn, P. Supaphol, P. Pavasant and D. Damrongsri, *Polym. Int.*, 2010, **59**(2), 227–235.
51 H. C. Anderson, J. B. Sipe, L. Hessle, R. Dhamyamraju, E. Atti, N. P. Camacho and J. L. Millán, *Am. J. Pathol.*, 2004, **164**(3), 841–847.
52 K. Wei, Y. Li, K. O. Kim, Y. Nakagawa, B. S. Kim, K. Abe, G. Q. Chen and I. S. Kim, *J. Biomed. Mater. Res., Part A*, 2011, **97**(3), 272–280.
53 C. H. Chen, M. F. Hsieh, Y. N. Ho, C. M. Huang, J. S. Lee, C. Y. Yang and Y. Chang, *J. Membr. Sci.*, 2011, **371**(1), 134–140.
54 J. A. Kaplan, R. Liu, J. D. Freedman, R. Padera, J. Schwartz, Y. L. Colson and M. W. Grinstaff, *Biomaterials*, 2016, **76**, 273–281.
55 C. S. Geetha, N. S. Remya, K. B. Leji, S. Syama, S. C. Reshma, P. J. Sreekanth, H. K. Varma and P. V. Mohanan, *Colloids Surf., B*, 2013, **112**, 204–212.
56 M. Jayabalan, K. T. Shalumon and M. K. Mitha, *J. Mater. Sci.: Mater. Med.*, 2009, **20**(6), 1379–1387.
57 S. Ghanaati, M. Barbeck, R. Detsch, U. Deisinger, U. Hilbig, V. Rausch, R. Sader, R. E. Unger, G. Ziegler and C. J. Kirkpatrick, *Biomed. Mater.*, 2012, **7**(1), 015005.
58 J. P. Fisher, D. Dean and A. G. Mikos, *Biomaterials*, 2002, **23**(22), 4333–4343.
59 X. Shao, J. C. H. Goh, D. W. Hutmacher, E. H. Lee and G. Zigang, *Tissue Eng.*, 2006, **12**(6), 1539–1551.
60 H. Xie, Z. Wang, L. Zhang, Q. Lei, A. Zhao, H. Wang, Q. Li, Z. Chen and W. Zhang, *PeerJ*, 2016, **4**(1), e2040.

